Model Silicone Elastomer Networks of High Junction Functionality: Synthesis, Tensile Behavior, Swelling Behavior, and Comparison with Molecular Theories of Rubber Elasticity

K. O. Meyers,* M. L. Bye, and E. W. Merrill

Department of Chemical Engineering, Massachusetts Institute of Technology, Cambridge, Massachusetts 02139. *Received January 17, 1980*

ABSTRACT: Multifunctional elastomeric networks of predetermined network chain density ν_s/V were prepared from α,ω-divinyl poly(dimethylsiloxane) (PDMS) chains (M_n ranging from 8800 to 52 000), the terminal vinyls of which were reacted with the silane hydrogens on linear and branched poly(methylsiloxanes) (PMHS) to give networks with high-functionality junctions, ϕ, ranging from 4 to 70. The stress–strain isotherms in elongation at 25 °C and the swelling ratios in benzene and oligomeric PDMS were measured for these networks. Network chain densities calculated from these measurements according to recent molecular theories of Flory were found to be substantially greater than the stoichiometric values. The elastic moduli/junction functionality trends observed were different from the trends predicted from these theories. The small-strain theory of Langley and Graessley gave good agreement with the experimental data.

The phenomena of rubber elasticity have been under investigation for over a century. Yet there still remains much controversy as to the correct molecular theory to explain elastomeric behavior. These theories relate an elastomer's network structure to its equilibrium mechanical properties. Verification of such relationships requires knowledge of network structure acquired independently of the theory under review. Unfortunately, classical network formation via radiation and chemical cross-linking results in elastomers with ill-defined network structure. Elastomers formed in this manner are limited in functionality, ϕ, to three or four and have network chains whose average molecular weight between chemical cross-links, M_c, is not precisely determinable from chemical measurements (e.g., by product gas evolution under irradiation). Furthermore, the distribution of molecular weights around M_c cannot be controlled independently of M_c. For these networks, structure may only be calculated through sol fraction, equilibrium moduli, and equilibrium degree of swelling, the last two requiring application of the same theory being investigated.

Many of these shortcomings may be alleviated by newer end-linking techniques. These techniques involve the reaction between difunctional polymer chains and plurifunctional junction sites to yield the desired network. This end-linking permits control of M_c and its dispersity via the number-average molecular weight and dispersity of the telechelic polymer. The functionality of the junction-site precursor, ϕ_0, dictates the final network functionality, and by going to *complete* reaction, loose ends can be eradicated. Thus, these techniques give rise to networks with a well-characterized "model" structure.

Until recently,[1-3] investigations utilizing model networks had been limited to functionalities of three or four.[4,5] Networks with higher functionality are predicted by various theories of rubber elasticity to display unique equilibrium tensile behavior (vide infra). As such, these multifunctional networks provide insight into the controversy surrounding these theories. The present study addresses the synthesis, equilibrium tensile behavior, and equilibrium swelling behavior of end-linked multifunctional poly(dimethylsiloxane) (PDMS) networks with known M_c and ϕ. This is accomplished by end-linking α,ω-divinyl PDMS with the silane hydrogens on linear and branched poly(methylsiloxanes) (PMHS)

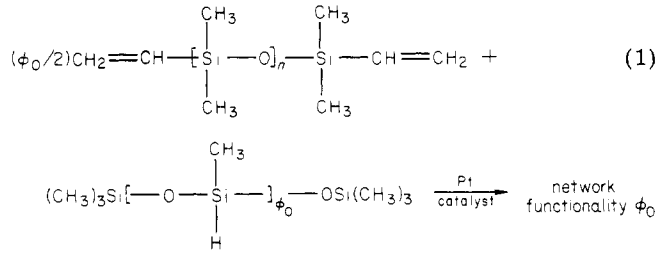

(1)

The functionality of the resultant network is governed by the molecular weight (functionality, ϕ_0) of the PMHS junction precursor. α,ω-Divinyl PDMS with molecular weights ranging from 9000 to 50 000 were reacted with a variety of linear and branched polyfunctional PMHS to prepare networks ranging in ϕ_0 from 4 to 84. The competing theories of rubber elasticity are evaluated in light of the equilibrium tensile behavior of these multifunctional networks.

Theory

The results of uniaxial stress–strain experiments are often analyzed in terms of the reduced stress defined by

$$[f] = f/[A(\alpha - \alpha^{-2})] \tag{2}$$

where f is the elastic force, A is the undeformed cross-sectional area, and α is the relative elongation defined by

$$\alpha = L/L_i \tag{3}$$

L being the length of the elongated sample and L_i its length when undeformed at the volume V of the deformed sample. For moderate values of simple extension, the empirical Mooney–Rivlin[6] relation

$$[f] = 2C_1 + 2C_2\alpha^{-1} \tag{4}$$

is found to hold quite satisfactorily. $2C_1$ and $2C_2$ are constants independent of strain.

Classical molecular theories of rubber elasticity[7,8] lead to an elastic equation of state which predicts the reduced stress to be constant over the entire range of uniaxial deformation. These theories may be divided into two groups. The first, referred to as the "affine" network theory,[7] assumes the network chains' end-to-end distance to obey Gaussian statistics. It further assumes the junctions in which the network chains terminate to be firmly embedded in the elastomeric matrix and as such undergo

* To whom correspondence should be addressed at ARCO Oil and Gas Co., Exploration and Productions Research Center, Dallas, Texas 75221.

0024-9297/80/2213-1045$01.00/0

displacements that are affine in the macroscopic strain. These assumptions lead to an elastic equation of state which may be written for simple elongation as[7]

$$[f] = \frac{\nu kT}{V}(V/V^0)^{2/3} \quad (5)$$

where T is the absolute temperature, k is the Boltzmann constant, V^0 is the volume in the undeformed state such that the mean-squared end-to-end length $\langle r^2 \rangle$ of a chain assumes the value $\langle r^2 \rangle_0$ for unperturbed, free chains, ν is the number of chains, and V is the volume of the network.

The second category of classical rubber elasticity theories also assumes the network chains to be Gaussian. Furthermore, the network chains are assumed to be "phantom" in nature; i.e., they are devoid of material properties and act only to impart force at the junctions in which their ends terminate.[8] This "phantom network" theory concludes that the mean positions of the junctions are affine in strain but that the fluctuations about these mean positions are invariant with strain. For simple elongation, the theory predicts[9]

$$[f] = \frac{\nu kT(V/V^0)^{2/3}}{V}(1 - 2/\phi) \quad (6)$$

wherein ϕ is the network functionality.

To explain the deviation between these classical theories and reality, Flory[9] and Ronca[10] have separately proposed a new model based on the supposition that in simple elongation, a network undergoes a transition between the two extremes of phantom and affine behavior. Flory's theory holds that in a real network, the fluctuations of a junction about its mean position may be significantly impeded by interactions with chains emanating from spatially, but not topologically, neighboring junctions. Thus, the junctions in a real network are more constrained than those in a phantom network. The elastic force is taken to be the sum of two contributions:[9]

$$f = f_{Ph} + f_c \quad (7)$$

f_{Ph} is the force predicted from a phantom network (eq 6) and f_c is the additional force arising from the aforementioned constraints on junction fluctuations. The theory[9] predicts that in simple elongation, the ratio f_c/f_{Ph} decreases with increasing strain and eventually goes to zero (phantom network) as α goes to infinity. Furthermore, at $\alpha = 1$, the theory predicts[9]

$$f_c/f_{Ph} \leq 2/(\phi - 2) \quad (8)$$

Therefore, Flory's theory concludes that as the functionality of a network increases, the constaint contribution, f_c, should decrease and eventually vanish. This follows from the fact that at high functionalities, the affine and phantom models are identical. Since $2C_2$ is indicative of the extent of the transition between the phantom and affine regimes (f_c), $2C_2$ is *predicted to be zero for high-functionality networks. Therefore, the large- and small-strain moduli should be identical for these high-functionality networks.*

The Flory theory considers topological interactions among junctions and chains only in that they restrict junction fluctuations. Ferry,[12] Langley,[14] and Dossin and Graessley[11] have argued that in small strain these interactions are also present along the chain contour and contribute to the modulus. Their conclusions are based on the rubbery plateau, G_N^0, which is observed for high molecular weight linear polymers in dynamic mechanical testing.[12,13] This plateau modulus is believed to be a measure of topological interactions or entanglements between chains. During network formation, a portion of these entanglements are permanently trapped, resulting in a small-strain modulus greater than that due to chemical cross-linking alone. Langley[14] expressed this as

$$G = G_c + G_e^{max}T_e \quad (9)$$

where G_c is the chemical contribution due to cross-linking and T_e is the proportion of the maximum concentration of topological interactions, G_e^{max}, which are permanently trapped by the network. Graessley[11,15] suggests that

$$G_c = \frac{\nu kT(1 - 2h/\phi)}{V} \quad (10)$$

where h is an empirical constant between one and zero, depending on the extent to which the junction fluctuations are impeded in the network ($h = 0$ for affine behavior, $h = 1$ for phantom behavior). Therefore[11,15]

$$G = \frac{\nu kT(1 - 2h/\phi)}{V} + G_e^{max}T_e \quad (11)$$

T_e is equivalent to the probability that any pair of interacting units are each part of elastically effective chains[14] and thus have all four chain ends terminated in a junction. Macosko[16] and Graessley[11,15,17] have developed the mathematical means of calculating T_e from sol data. G_e^{max} is expected to be closely related to G_N^0.

Thus eq 11 predicts a small-strain modulus greater than that predicted by the Flory theory due to the $G_e^{max}T_e$ term. To test the predictions and discrepancies of these two theories of rubber elasticity, we have prepared multifunctional networks with known ϕ, ν/V, and T_e. Our experimental procedures and results are summarized in the following sections.

Experimental Section

Multifunctional poly(dimethylsiloxane) (PDMS) networks were prepared via the addition of a silane hydrogen on poly(methylsiloxanes) (PMHS) to vinyl-terminated linear PDMS polymers in the presence of *cis*-dichlorobis(diethyl sulfide)platinum(II) catalyst (see eq 1). For functionalities between 6 and 84, linear and branched PMHS were used as junction sites. A commercial linear PMHS (Aldrich Chemical Co.), $M_n \sim 3000$, was repeatedly fractionated from toluene with nitromethane to obtain four narrow molecular weight cuts. The linear PMHS was also extended by reaction with divinyltetramethyldisiloxane (ViD_2Vi). The reaction was conducted in a 50 wt % toluene solution in the presence of a 20-ppm Pt catalyst under argon with constant stirring at room temperature for 96 h. A 4:1 PMHS/ViD_2Vi mole ratio was utilized. The resulting high molecular weight polymer was fractionated repeatedly from toluene with dimethyl sulfoxide (Me_2SO) to obtain two narrow molecular weight cuts.

Branched PMHS were synthesized by reacting $[H(CH_3)SiO]_4$, tetramethylcyclotetrasiloxane, D_4', with ViD_2Vi. The reactions were conducted in 50% toluene in the presence of 20-ppm Pt catalyst under argon with constant stirring at room temperature for 96 h. D_4'/ViD_2Vi molar ratios of 1.4, 1.7, and 2.0 were utilized. The resulting broad-dispersity branched PMHS were fractionated repeatedly from toluene with Me_2SO to yield three narrow molecular weight fractions. The branched and linear PMHS fractions were dissolved in hexane, extracted repeatedly with nitromethane, and filtered. The hexane was stripped off in a rotary evaporator. The polymers were evacuated at 70 °C for at least 96 h.

The molecular weight distributions of the six linear and three branched PMHS were determined by size exclusion chromatography (GPC). Narrow molecular weight distribution polystyrenes were used as calibration standards. The number-average molecular weights of the PMHS were measured via vapor phase osmometry (VPO). The molal silane hydrogen concentrations (equivalent weight, E_j) of the PMHS were determined spectrophotometrically, using the silane hydrogen stretching frequency in the infrared at 2174 cm^{-1}. The absorbance measurements were

Table I
PMHS Characterization Data

ϕ_0	M_n	E_j	M_w/M_n
	Linear		
6.65	650	97.7	1.24
21.5	1460	68.1	1.42
33.0	2130	64.5	1.57
43.9	2780	63.4	1.60
58.4	3710	63.4	1.71
83.6	5260	62.9	1.66
	Branched		
10.5	1590	151.6	1.47
23.8	4610	193.6	1.43
38.1	7480	196.2	1.50

conducted in carbon tetrachloride solution using a Digilab Fourier transform infrared spectrophotometer, Model 14. Tetramethylcyclotetrasiloxane (Rhône-Poulenc, 99+%) and heptamethylcyclotetrasiloxane (Silar Labs, 99+%) were used as calibration standards. The functionality of the junction precursor, ϕ_0, is the quotient of M_n and E_j. Table I summarizes these data for the PMHS polymers. For tetrafunctional networks [H-Si$(CH_3)_2$O]$_4$Si was utilized as the junction site.[29]

Two sets of α,ω-divinyl PDMS were used in this study. The first set consisted of commercially available polymers which were supplied by General Electric[21] and Dow Corning.[22] Four different number-average molecular weight α,ω-divinyl PDMS were provided: M_n = 8800, M_n = 11 100, M_n = 21 600, and M_n = 28 100. Four additional number-average molecular weights of α,ω-divinyl PDMS were obtained by combining that pair of the supplied α,ω-divinyl PDMS with M_n closest to the desired M_n.

The second set of α,ω-divinyl PDMS was synthesized by the anionic ring-opening polymerization of hexamethylcyclotrisiloxane by the difunctional initiator dilithium stilbene (eq 12). This living

$$(2a/3)[(CH_3)_2SiO]_3 + x\text{LiCH(Ph)CH(Ph)Li} \xrightarrow[25\ ^\circ C]{THF} x\text{Li}[\text{OSi}(CH_3)_2]_{a/x}CH(\text{Ph})\text{CH(Ph)}[\text{Si}(CH_3)_2\text{O}]_{a/x}Li \quad (12)$$

polymer was capped with vinyldimethylchlorosilane to give the desired product (eq 13). The details of the synthesis procedure

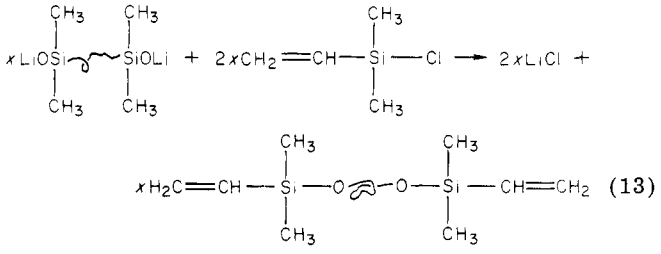

are given elsewhere.[31] α,ω-Divinyl PDMS with 14 different values of M_n ranging from 12 200 to 52 800 were synthesized for this study. The anionic polymerization resulted in α,ω-divinyl PDMS with relatively narrow molecular weight distributions (M_w/M_n = 1.08–1.30).

The molecular weight distributions (M_w/M_n) of all the α,ω-divinyl PDMS were determined by GPC. Universal calibration curve theory was applied to determine the M_n of the polymers. Additionally, the number-average molecular weights were determined by titration of the vinyl end groups with mercuric acetate.[19,22] Vinyl concentration in the α,ω-divinyl PDMS was also measured spectrophotometrically by using the C=C stretching frequency at 4650 cm^{-1}. Absorbance measurements were conducted neat in a Cary 14 spectrophotometer. Ten thousand molecular weight PDMS was used as the reference material. ViD$_2$Vi (99+% pure, Rhône-Poulenc Co.) was used as a calibration standard. Good agreement (+5%) between the two techniques was obtained for the α,ω-divinyl PDMS provided by General Electric and that synthesized with narrow molecular weight distribution. However, the latter technique was not applicable to the Dow Corning materials because of the presence of two interfering peaks at 4580 and 4610 cm^{-1}. These peaks are believed to be due to SiC_6H_5 groups present in these polymers. The M_n by GPC and the M_n by vinyl determination as well as

Table II
Commercial α,ω-Divinyl PDMS Characterization Data

M_n(vinyl)	M_n(GPC)	M_w/M_n[a]	w_n[b]
8 800	8 300	2.34	2.7
11 100	9 900	2.20	3.0
21 600	16 000	2.18	3.3
28 100	18 300	2.06	3.4
10 100	9 200	2.28	2.9
12 900	11 100	2.46	3.1
17 000	13 600	2.37	3.2
25 300	17 300	2.13	3.3

[a] Corrected for nonreactive oligomeric PDMS. [b] Wt % nonreactive oligomeric PDMS.

Table III
Narrow Molecular Weight Distribution α,ω-Divinyl PDMS Characterization Data

M_n(vinyl)	M_n(GPC)	M_n(osmometry)	M_w/M_n
12 200	12 900	11 900	1.09
13 900	13 200		1.18
14 300	13 100	15 100	1.15
15 200	15 300	14 700	1.17
17 400	16 500	16 500	1.31
18 300	17 300		1.19
22 000	20 300		1.17
25 300	24 300		1.26
27 500	28 200		1.08
29 500	31 800		1.11
41 700	40 100	39 800	1.27
48 400	48 400	50 700	1.26
51 000	53 200	53 600	1.07
52 800	52 600	50 100	1.12

the M_w/M_n are given in Table II for the commercial polymers and in Table III for the narrow molecular weight distribution α,ω-divinyl PDMS. The number-average molecular weights determined by osmometry are also given in Table III. Excellent agreement is found among the number-average molecular weights as measured by GPC, osmometry, and vinyl end group analysis.

The discrepancy between the M_n by GPC and that by vinyl measurements for the *commercial* α,ω-divinyl PDMS is due to the presence of approximately 3% nonreactive low molecular weight PDMS in all eight of the commercial α,ω-divinyl PDMS. The presence of this low molecular weight material was confirmed by reacting the α,ω-divinyl PDMS with a twofold excess of ϕ_0 = 43.9 PMHS. The sol of the resulting network was analyzed by GPC and found to contain only a low molecular weight PDMS (M_n ~1200). Additionally, this sol was analyzed for vinyl groups by the spectrophotometric technique and no vinyl groups were determined. Table II lists the percentage of nonreactive oligomer found in each of the commercial α,ω-divinyl PDMS polymers, w_n.[32] No nonreactive oligomeric PDMS was found in the narrow molecular weight distribution α,ω-divinyl PDMS.

The *cis*-dichlorobis(diethyl sulfide)platinum(II) catalyst was prepared following the procedure described in ref 18. The resulting yellow crystals were dissolved in toluene to give a 1.5 wt % solution. The two network precursors were combined with sufficient catalyst to give an overall Pt concentration of 20 ppm. The liquid mixture, after being mixed with a mechanical stirrer, was poured into rectangular acrylate molds, degassed, and cured at 75 °C under argon for 5 days to ensure complete reaction. The resulting films had a thickness of 1–2 mm. An excess of silane hydrogen was utilized to ensure complete reaction of the vinyl end groups.[30]

Samples of each network formed were extracted with benzene to determine the mass fraction of polymer not incorporated into the network, w_e. The molecular weight distribution of each sol was determined by GPC. For the networks prepared from the eight *commercial* α,ω-divinyl PDMS (see Table II), these distributions were bimodal with a small high molecular weight peak due to the unreacted α,ω-divinyl PDMS and a large low molecular weight peak due to nonreactive low molecular weight PDMS (see Figure 1). The ratio of the α,ω-divinyl PDMS peak area to the total area was multiplied by w_e to arrive at w_s, the corrected sol due only to *unreacted* α,ω-divinyl PDMS. The GPC of sols from

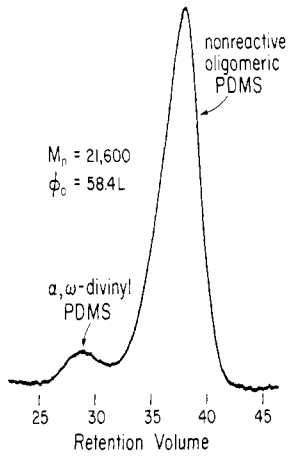

Figure 1. Gel permeation chromatography of the sol from a M_n = 21 600 commercial α,ω-divinyl PDMS, ϕ_0 = 58.4 linear network. Bimodal distribution arises from the nonreactive oligomeric PDMS.

the networks prepared with the narrow distribution α,ω-divinyl PDMS (see Table III) displayed but a single peak due to the unreacted α,ω-divinyl PDMS ($w_e = w_s$). The shape and position of this single peak in the molecular weight distribution of the sol were identical with that of the narrow molecular weight distribution α,ω-divinyl PDMS used to prepare the network.

Equilibrium swelling in benzene was also determined for each network by using standard procedures.[20] Additionally, the equilibrium swelling of each network in an oligomeric PDMS (M_n = 1170 by VPO) was measured. In both cases, the volume fraction of polymer at equilibrium swelling, v_{2m}, was calculated assuming additivity of volumes.

Equilibrium tensile stress–strain isotherms were obtained at 25 °C on dumbbell-shaped specimens (3 × 1 × 0.1 cm test regions) cut from unextracted films of the network. Samples were stressed by hanging different weights. Elongation was measured with a Gaertner cathetometer between two marks 2.9 cm apart. Measurements were made in a sequence of increasing elongations with frequent values taken out of sequence to check reproducibility. The data were fit to a Mooney–Rivlin plot with a linear least-squares regression. Reproducibility of the synthesis techniques was often checked by preparing duplicate films of a network and comparing their stress–strain isotherms. The precision of the testing procedures was checked by running duplicate or triplicate samples from the same film. In both cases, good agreement was obtained ($2C_1$, $2C_2$: ±5%). For every network, *at least three* samples were tested, and the *average* $2C_1$ and $2C_2$ are reported in the figures and tables which follow. In general, the standard deviation of these average moduli was ±5%.

The characterization data obtained from the networks prepared for this study are summarized in Tables IV and V. Listed are the M_n of the α,ω-divinyl PDMS used, the functionality of the PMHS junction precursor used, the molar ratio of silane hydrogen to vinyl (R), values of w_s, w_e, v_{2m} in benzene, and v_{2m} in oligomeric PDMS, the *average* values of $2C_1$ and $2C_2$, and the ratio $2C_2/2C_1$. The data for networks prepared from the commercial α,ω-divinyl PDMS are given in Table IV. The data for networks prepared using the narrow molecular distribution α,ω-divinyl PDMS are given in Table V. For these latter networks, $w_e = w_s$.

Results and Discussion

Figure 2 is a plot of stress–strain data for ϕ_0 = 4 and 43.9 networks formed with the M_n = 21 600 commercial α,ω-divinyl PDMS.[36] The stress–strain isotherms are plotted as reduced stress (in MPa) vs. reciprocal elongation and are typical of all the networks tested in this study in their excellent agreement with the empirical Mooney–Rivlin relationship. Although the two stress–strain isotherms in Figure 2 are for networks of drastically different functionalities, they appear to have the same slope, $2C_2$. Furthermore, the network of functionality ϕ_0 = 43.9 has an intercept, $2C_1$, approximately twice as great as that of

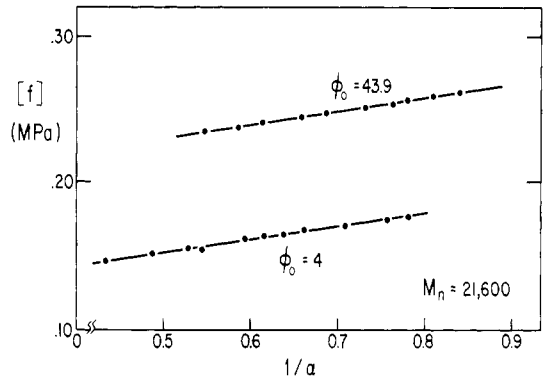

Figure 2. Representative stress–strain isotherms of the end-linked PDMS networks obtained in elongation at 25 °C.

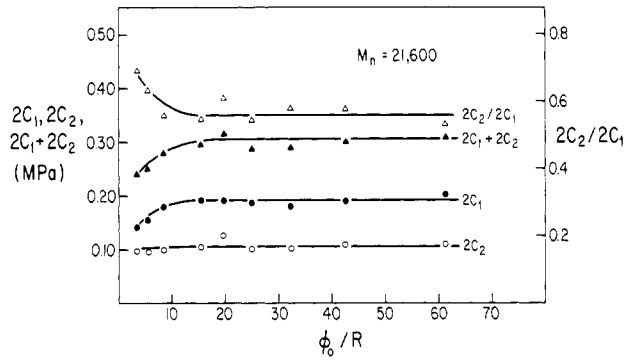

Figure 3. Dependence of $2C_1$, $2C_2$, $2C_1 + 2C_2$, and $2C_2/2C_1$ on network functionality for M_n = 21 600 PDMS networks.

the tetrafunctional network. According to the Flory theory,[9] the higher functionality network should have a lower $2C_2$. This discord between experiment and theoretical prediction is further explored in Figure 3.

In Figure 3, $2C_1$, $2C_2$, $2C_1 + 2C_2$, and $2C_2/2C_1$ are plotted against the functionality of the PMHS junction precursor, ϕ_0, divided by the molar ratio of silane hydrogen to vinyl used in forming the networks, R. This quotient was used instead of ϕ_0 to correct the functionality of the PMHS junction precursor for the fact that an excess of junction precursor ($R > 1$) had been used in forming the networks to ensure complete reaction of the vinyl groups ($\phi \sim \phi_0/R$). All the networks represented in Figure 3 were made with the M_n = 21 600 α,ω-divinyl PDMS. $2C_1$ and $2C_1 + 2C_2$ are found to increase with increasing network functionality in the low-functionality region (4–10); however, further increases in functionality beyond 20 result in little change in these moduli. A prediction of the Flory theory is that in the limit of large strain ($\alpha^{-1} \to 0$), the network will exhibit phantom behavior. Thus, the infinite-strain modulus would increase as $1 - 2/\phi$ with functionality from $\nu kT/2V$ at $\phi = 4$ to $0.9\nu kT/V$ at $\phi = 20$. Increasing ϕ to infinity would result in only a 10% further increase in the phantom modulus. $2C_1$, being an extrapolation from finite to infinite strain, overestimates the phantom modulus but the trend should remain the same. Therefore, the increase in $2C_1$ qualitatively follows the Flory predictions.

The ratio $2C_2/2C_1$ decreases asymptotically with increasing ϕ_0/R. Once again the majority of the decrease occurs between four and ten. $2C_2$, being a measure of the magnitude of the transition between phantom and affine behavior, is predicted by the Flory theory to decrease asymptotically with increasing functionality, as is $2C_2/2C_1$. The theoretical asymptote for both is *zero*. The experimentally determined limit for $2C_2$ was found to be 0.11 MPa for the M_n = 21 600 networks. For $2C_2/2C_1$, an asymptote of 0.56 was observed. Both of these values are

Table IV
Network Characterization Data: Networks Prepared Using Commercial α,ω-Divinyl PDMS

M_n	ϕ_o [a]	R	$10^2 w_e$	$10^2 w_s$	v_{2m} benzene	v_{2m} PDMS	$2C_1$, MPa	$2C_2$, MPa	$2C_2/2C_1$
8 800	4	1.005	3.62	0.49	0.316	0.421	0.244	0.084	0.344
8 800	23.8 B	1.199	2.70	0.15	0.396	0.394	0.390	0.087	0.223
8 800	43.9 L	1.114	2.89	0.17	0.391	0.518	0.360	0.130	0.361
10 100	23.8 B	1.203	2.99	0.20	0.381	0.513	0.408	0.062	0.152
10 100	43.9 L	1.268	3.01	0.17	0.380	0.507	0.373	0.078	0.209
11 100	4	1.100	2.94	0.12	0.300	0.401	0.207	0.087	0.420
11 100	6.7 L	1.196	3.66	0.61	0.320	0.433	0.246	0.065	0.264
11 100	10.5 B	1.249	3.78	0.52	0.344	0.467	0.298	0.074	0.248
11 100	21.5 L	1.394	3.08	0.14	0.360	0.501	0.358	0.083	0.232
11 100	23.8 B	1.201	2.87	0.15	0.358	0.492	0.377	0.061	0.162
11 100	33.0 L	1.298	3.12	0.13	0.364	0.488	0.375	0.060	0.160
11 100	38.1 B	1.200	3.68	0.53	0.360	0.501	0.351	0.052	0.148
11 100	43.9 L	1.201	3.41	0.45	0.355	0.468	0.316	0.053	0.168
11 100	58.4 L	1.296	3.41	0.26	0.362	0.485	0.355	0.054	0.152
11 100	83.6 L	1.351	3.21	0.14	0.366	0.491	0.361	0.065	0.180
11 100	83.6 L	1.351	3.21	0.14	0.366	0.491	0.361	0.065	0.180
12 900	23.8 B	1.202	3.20	0.28	0.350	0.467	0.306	0.078	0.255
12 900	43.9 L	1.298	3.29	0.21	0.350	0.465	0.277	0.097	0.350
17 000	23.8 B	1.197	3.26	0.27	0.321	0.434	0.232	0.097	0.418
17 000	43.9 L	1.308	3.45	0.19	0.320	0.431	0.216	0.113	0.523
21 600	4	1.121	3.52	0.49	0.270	0.365	0.142	0.098	0.690
21 600	4	1.121	3.52	0.49	0.270	0.365	0.142	0.098	0.690
21 600	6.7 L	1.204	4.02	0.73	0.268	0.365	0.153	0.096	0.627
21 600	10.5 B	1.247	4.30	0.49	0.297	0.392	0.180	0.101	0.561
21 600	21.5 L	1.399	3.12	0.18	0.318	--	0.191	0.105	0.550
21 600	23.8 B	1.209	3.06	0.22	0.308	0.419	0.191	0.126	0.660
21 600	33.0 L	1.316	3.89	0.36	0.304	0.397	0.186	0.102	0.548
21 600	38.1 B	1.216	4.06	0.51	0.310	0.351	0.200	0.088	0.440
21 600	43.9 L	1.359	3.73	0.38	0.304	0.399	0.180	0.104	0.578
21 600	58.4 L	1.375	3.59	0.25	0.313	0.406	0.191	0.110	0.576
21 600	83.6 L	1.364	3.37	0.41	0.310	0.410	0.201	0.108	0.537
25 300	23.8 B	1.646	3.89	0.83	0.291	0.384	0.165	0.082	0.497
28 100	23.8 B	1.164	3.21	0.12	0.297	0.397	0.177	0.121	0.687
28 100	43.9 L	1.450	3.90	0.33	0.297	0.383	0.175	0.109	0.623

[a] B = branched PMHS; L = linear PMHS.

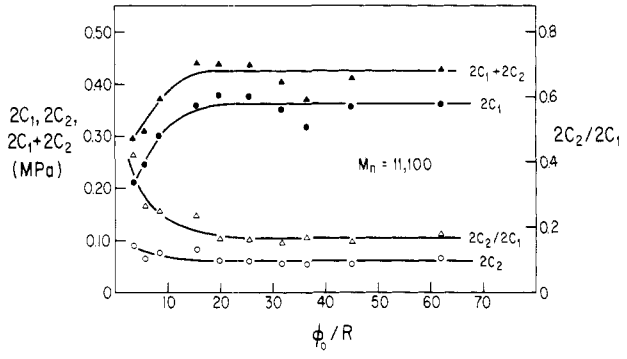

Figure 4. Dependence of $2C_1$, $2C_2$, $2C_1 + 2C_2$, and $2C_2/2C_1$ on network functionality for M_n = 11 100 PDMS networks.

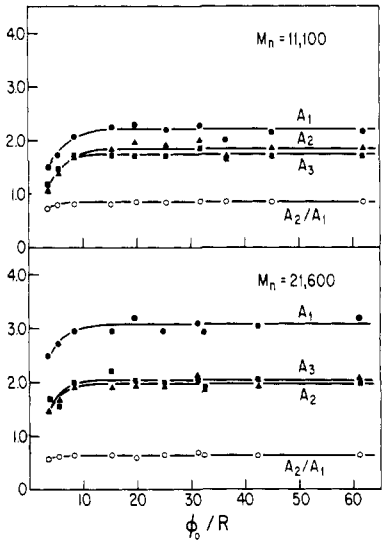

Figure 5. Dependence of the structure factors A_1, A_2, and A_3 and the ratio A_2/A_1 on network functionality for the M_n = 21 600 and 11 100 networks.

significantly greater than the zero prediction. Examination of Figure 3 indicates that these nonzero values cannot be attributed to experimental error since the five networks with $\phi_0/R \geq 20$ gave little scatter from the asymptotes. Furthermore, each point in Figure 3 is an average of three or more tensile tests. Further disagreement between theory and experiment is seen in the general $2C_2$ behavior. Experimentally, $2C_2$ is found to remain constant with increasing functionality rather than to decrease as predicted by the Flory theory.

Figure 4 is a plot of the various moduli against ϕ_0/R for networks formed with the M_n = 11 100 commercial α,ω-divinyl PDMS. Similar behavior to the M_n = 21 600 networks is observed for $2C_1$, $2C_2$, $2C_1/2C_2$, and $2C_1 + 2C_2$. The ratio $2C_2/2C_1$ decreases to a limit of 0.17 with increasing functionality and $2C_2$ remains constant with increasing functionality. As with the M_n = 21 600 networks, $2C_2/2C_1$ and $2C_2$ are significantly nonzero at high functionalities and, as such, disagree with the theoretical predictions of Flory.

The asymptotic values of $2C_1$ and $2C_1 + 2C_2$ in Figures 3 and 4 also disagree in *magnitude* with the theoretical predictions of Flory. These results are quantified in terms of the structure factors A_1 and A_2 and the ratio A_2/A_1 plotted against functionality in Figure 5. A_1 and A_2 relate the small- and large-strain moduli to the number of net-

Table V
Network Characterization Data: Networks Prepared Using Narrow Molecular Weight Distribution α,ω-Divinyl PDMS

M_n	ϕ_0[a]	R	$10^2 w_s$	v_{2m} benzene	v_{2m} PDMS	$2C_1$, MPa	$2C_2$, MPa	$2C_2/2C_1$
12 200	23.8 B	1.255	0.18	0.354		0.325	0.078	0.240
12 200	43.9 L	1.295	0.37	0.349		0.316	0.070	0.222
13 900	23.8 B	1.650	0.64	0.310	0.443	0.225	0.065	0.289
13 900	58.4 L	1.797	0.95	0.335	0.458	0.253	0.075	0.296
14 300	23.8 B	1.285	0.42	0.340		0.250	0.097	0.388
14 300	43.9 L	1.304	0.48	0.335		0.255	0.094	0.369
15 200	23.8 B	1.300	0.52	0.335	0.450	0.268	0.091	0.340
15 200	43.9 L	1.803	0.69	0.338	0.457	0.212	0.127	0.599
17 400	23.8 B	1.652	0.53	0.294	0.401	0.200	0.056	0.280
18 300	43.9 L	1.798	0.67	0.326	0.430	0.242	0.065	0.269
22 000	23.8 B	1.308	0.19	0.302		0.198	0.114	0.576
22 000	43.9 L	1.348	0.35	0.305		0.193	0.106	0.549
25 300	43.9 L	1.799	0.64	0.300	0.340	0.196	0.059	0.301
27 500	23.8 B	1.358	0.31	0.295		0.174	0.091	0.523
27 500	43.9 L	1.391	0.42	0.295		0.173	0.101	0.584
29 500	23.8 B	1.342	0.26	0.292		0.170	0.101	0.594
29 500	43.9 L	1.403	0.58	0.293		0.164	0.082	0.500
41 700	23.8 B	1.649	0.88	0.268	0.370	0.129	0.101	0.783
48 400	23.8 B	1.666	0.90	0.280		0.168	0.043	0.256
51 000	23.8 B	1.417	0.76	0.257		0.106	0.105	0.991
52 800	23.8 B	1.402	0.71	0.248		0.094	0.098	1.043
52 800	43.9 L	1.517	0.97	0.251		0.082	0.094	1.146

[a] B = branched PMHS; L = linear PMHS.

work chains per unit volume calculated from stoichiometry, ν_s/V

$$2C_1 + 2C_2 = \frac{A_1 \nu_s kT}{V}(V/V^0)^{2/3} \quad (14)$$

$$2C_1 = \frac{A_2 \nu_s kT}{V}(V/V^0)^{2/3} \quad (15)$$

According to the Flory theory,[9] the predicted range on A_1 and A_2 lies between one and $1 - 2/\phi$. The upper limit, unity, corresponds to affine behavior and the lower limit occurs in phantom behavior. Therefore both A_1 and A_2 *have predicted asymptotes of 1 at high functionalities.*

For $\phi_0 > 10$, ν_s/V was calculated from the extent of reaction of the vinyl groups, ϵ, in the following manner:

$$\frac{\nu_s}{V} = \frac{\epsilon^2 \rho}{M_n + 2RE_j} \quad (16)$$

where M_n is the number-average molecular weight of the α,ω-divinyl PDMS, ρ is the density of the network (ρ = 0.972 g/cm^3), E_j is the equivalent weight of the PMHS junction precursor, and R is the stoichiometric ratio of the reactants. For lower functionality networks the relations derived by Miller and Macosko[23] were utilized to calculate ν_s/V. The ϵ^2 in eq 16 accounts for incomplete reaction of the networks. For the majority of networks formed in this study, $\epsilon \geq 0.95$. However, even at $\epsilon = 0.95$, ϵ^2 results in a 10% decrease in ν_s/V over that calculated assuming complete reaction. For $\phi_0 > 10$, ϵ was obtained from the corrected sol fraction, w_s

$$w_s = \frac{(1 - \epsilon)^2 M_n}{M_n + 2RE_j} \quad (17)$$

Equation 17 assumes that only reacted α,ω-divinyl PDMS can be extracted from the network; i.e., all the PMHS junction precursor is reacted into the network. This assumption would result in less than 1% error for $\phi_0 > 10$ and $\epsilon > 0.8$.

Using ν_s/V, A_1 and A_2 were calculated from eq 14 and 15 ($V = V^0$) and are plotted against ϕ_0/R in Figure 5 for both the M_n = 11 100 and 21 600 networks. For a phantom network, a twofold asymptotic increase in A_2 is predicted as the functionally increases from four to infinity. Although $2C_1$ overestimates this phantom modulus, the Flory theory would predict an approximate twofold increase in A_2 for a real network. The small-strain modulus, $2C_1 + 2C_2$, would be expected to behave more affinely as functionality is increased and, therefore, A_1 would be predicted to increase asymptotically with increasing functionality but to a lesser extent than A_2. These predicted trends in the structure factors are observed in Figure 5. However, the absolute magnitude of the asymptotes in A_1 and A_2 are two- to threefold greater than the Flory theoretical predictions ($A_1 = A_2 = 1$).

The ratio $A_2/A_1 = 2C_1/(2C_1 + 2C_2)$ is also plotted in Figure 5. The low-functionality values are in accord with theory; however, the predicted high-functionality asymptote of 1 is not reached. The limiting values of A_2/A_1 obtained are 0.63 and 0.86, respectively, for networks having chains of 21 600 and 11 100 molecular weight.

A third structure factor is also plotted in Figure 5, A_3. A_3 is the ratio of network chain density calculated from affine equilibrium swelling theory to that obtained from stoichiometry

$$A_3 = \frac{-\{\ln(1 - v_{2m}) + v_{2m} + \chi_1 v_{2m}^2\} v_{2r} V_0}{V_1 \nu_s (v_{2m}^{1/3} v_{2r}^{2/3} - 2R v_{2m}/\phi)} \quad (18)$$

where $v_{2r} = (V_d/V_0)$ (V_d is the volume of the dried extracted network), V_1 is the molar volume of the solvent, and χ_1 is the polymer–solvent interaction parameter.[7] The equilibrium degree of swelling in benzene, v_{2m}, was used in the calculation of A_3. χ_1 was obtained as a function of volume fraction polymer from published results.[24] Good agreement between A_2 and A_3 was obtained for both the M_n = 11 100 and 21 600 networks in Figure 5.

The three structure factors in Figure 5 are independent of network functionality for ϕ_0/R greater than ten. However, a comparison of the networks having chains of M_n = 11 100 and M_n = 21 600 indicates the chain molecular weight has a significant effect on these structure factors. This effect is explored in greater detail in Figure 6, which plots A_1, A_2, and A_3 against ν_s/V for all of the networks prepared in this study with $\phi_0 > 10$. The open symbols refer to networks prepared using the narrow molecular

weight distribution α,ω-divinyl PDMS (Table V) and the filled symbols refer to those networks prepared using the commercial α,ω-divinyl PDMS (Table IV). At these high functionalities, the Flory theory would predict all three structure factors to have the asymptotic value of 1 and to be independent of ν_s/V. The data in Figure 6 clearly do not support these predictions.

Excellent agreement between the value of ν_s/V calculated from affine swelling theory (A_3) and ν_s/V calculated from $2C_1$ (A_2) is observed in Figure 6 for all of the high-functionality networks in this study. Furthermore, good agreement is observed in Figure 6 between the values of structure factors for networks formed using commercial α,ω-divinyl PDMS and the values of the structure factors for networks formed using the narrow molecular weight distribution α,ω-divinyl PDMS. This suggests that network chain length distribution had negligible effect on the equilibrium tensile behavior for the range of M_w/M_n investigated in this study (M_w/M_n = 1.1–2.5). Mark[33] has made a similar observation for tetrafunctionally end-linked PDMS networks.

In low-functionality networks (3 or 4), Andrady et al.[25] have postulated that decreasing the network chain molecular weight would be expected to decrease the degree of topological interpenetration of junctions. At very high ν_s/V, the short network chains would result in the close spatial proximity of topologically neighboring junctions. Thus, the Flory theory would predict increasing phantom behavior over the entire range of strain with increasing ν_s/V. Correspondingly, the structure factors A_1 and A_2 should decrease asymptotically to $1 - 2/\phi$ with increasing ν_s/V, with A_1 decreasing more rapidly than A_2. Therefore, A_2/A_1 should approach a limit of 1 with increasing ν_s/V.

These trends in A_1, A_2, and A_2/A_1 with ν_s/V predicted and observed[35] for networks of low functionality are also observed for the high-functionality networks in Figure 6. However, as in Figure 5, the magnitudes of the individual structure factors are *2–5 times greater* than the theoretical predictions. A common asymptote at large ν_s/V is observed for A_1, A_2, and A_3 at approximately 1.75.

The similarity of trends in ν_s/V of the high-functionality networks in Figure 6 with those of low-functionality networks could lead to the hypothesis that the high-functionality networks are effectively trifunctional

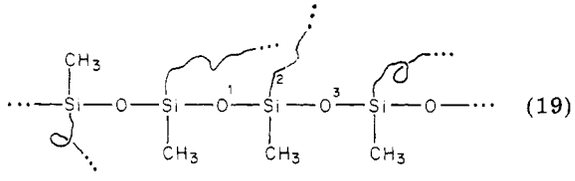

(19)

Each "trifunctional" junction would have two extremely short chains and one long chain emanating from it. According to such a hypothesis, the nonzero values of $2C_2$ and $2C_2/2C_1$ observed in Figures 3 and 4 are to be expected. Furthermore, the effective number of network chains would be about 3 times the value calculated via eq 16, resulting in a threefold decrease in A_1, A_2, and A_3. The magnitudes of these corrected structure factors would be more in accord with the Flory theory predictions for trifunctional networks. However, the hypothesis hardly seems reasonable in that the two 2–3 bond short chains in eq 19 would have to be treated as elastic chains. Furthermore, the value of A_1 at low ν_s/V would still be twofold greater than the limits of unity predicted by the Flory theory.

The magnitude of A_1 in Figures 5 and 6 can, alternatively, be explained by an entanglement contribution to

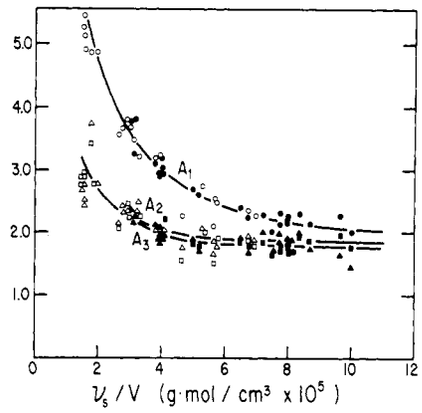

Figure 6. Dependence of the structure factors A_1 (●), A_2 (▲), and A_3 (■) on the stoichiometric network chain concentrations. Networks formed using the commercial α,ω-divinyl PDMS are represented by filled symbols. Networks formed using the narrow molecular weight distribution α,ω-divinyl PDMS are represented by open symbols.

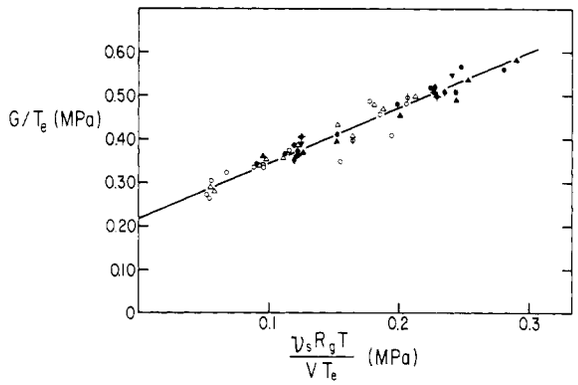

Figure 7. Langley–Graessley plot for networks with $\phi_0 > 10$. Filled symbols refer to the commercial α,ω-divinyl PDMS networks. Open symbols refer to the narrow molecular weight distribution α,ω-divinyl PDMS networks. Functionality (ϕ_0): 10.58 (■), 21.5 L (♦), 23.8 B (●), 33.0 L (●), 38.1 B (▼), 43.9 L (▲), 58.4 L (●), and 83.6 (●) (R_g = gas constant).

the small-strain modulus. According to eq 11 and 14, for $\phi_0/R > 10$ and $G \cong 2C_1 + 2C_2$

$$A_1 = \frac{GV}{\nu_s kT} = 1 + \frac{T_e G_e^{max} V}{\nu_s kT} \qquad (20)$$

Thus Graessley's[11] small-strain theory would suggest that A_1 for these high-functionality networks should increase without limit as the value of ν_s/V is decreased. A plot of G/T_e vs. $\nu_s kT/T_e V$ (Figure 7) was made to test if the small-strain data of the high-functionality networks could be represented by the Graessley theory. $2C_1 + 2C_2$ was used to approximate the small-strain modulus. This approximation can lead to slightly higher G values due to curvature in the Mooney–Rivlin plots at small extensions. However, from the data, this error appears to be less than 5%. T_e of the high-functionality networks was taken to be ϵ^4, where ϵ was calculated from eq 17. The small-strain modulus data of all of the networks prepared in this study with $\phi_0 > 10$ are plotted in Figure 7. The data were fitted by linear regression to a single line having a slope of 1.27 and an intercept of 0.215 MPa.

Graessley predicts the slope of such a plot to be equivalent to $1 - 2h/\phi$. Networks with functionalities greater than ten would therefore have a slope of unity. As indicated in Figure 7, there is good agreement between the theoretical and experimental slopes. The intercept of 0.215 MPa obtained in Figure 7 should be equivalent to G_e^{max}.

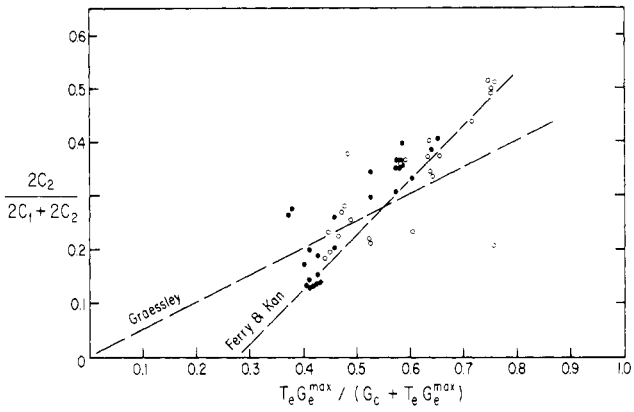

Figure 8. The ratio $2C_2/(2C_1 + 2C_2)$ as a function of $G_e^{max}T_e/(G_c + G_eT_e^{max})$. Filled symbols are for commercial α,ω-divinyl PDMS networks and open symbols are for narrow molecular weight distribution α,ω-divinyl PDMS networks.

Experimental values of 0.20 and 0.23 MPa for G_e^{max} have been reported[4] for trifunctional and tetrafunctional networks, respectively. Additionally, G_e^{max} should be close to G_N^0. Literature values of 0.24,[4] 0.20, and 0.29 MPa[27,28] have been reported for G_N^0. The intercept of Figure 7 is in excellent agreement with both the literature values of G_e^{max} for trifunctional and tetrafunctional PDMS networks and the reported values of G_N^0. Therefore, the slope and intercept of Figure 7 are in good agreement with the theoretical predictions of Graessley. The excellent fit of the *eight different network functionalities* to the single line of Figure 7 is further evidence of the agreement between the small-strain data and Graessley's theory.

In Figure 6, it is clearly demonstrated that $2C_1$ (A_2) is considerably greater than $\nu_s kT/V$ ($A_2 = 1$). Ferry and Kan,[34] Dossin and Graessley,[11] and Pearson and Graessley[15] have suggested trapped entanglements as a possible contribution to $2C_1$ and $2C_2$. Their results can be represented as

$$\frac{2C_2}{2C_1 + 2C_2} = A + B\frac{T_eG_e^{max}}{T_eG_e^{max} + G_c} \qquad (21)$$

or in terms of $2C_1$ as

$$2C_1 = G_c(1 - A) + (1 - A - B)T_eG_e^{max} \qquad (22)$$

Ferry and Kan[34] found $A = -0.275$ and $B = 1$ for a variety of tetrafunctional networks. Dossin and Graessley[11] reported $B = 0.5$ and $A = 0$ for tetrafunctional polybutadiene networks. In Figure 8 the data of the high-functionality networks prepared in this study have been plotted as suggested by eq 21 using the value of G_e^{max} as determined in Figure 7. The correlations suggested by Ferry–Kan and Graessley–Dossin are also drawn in Figure 8.

There is a good deal of scatter in the data but better agreement is observed with the Ferry–Kan correlation than with that of Dossin and Graessley. The data suggest smaller values of $(-A)$ and B than those reported by Ferry and Kan.

Conclusions

The stress–strain behavior and the equilibrium swelling behavior of the high-functionality networks prepared in this study differ markedly from the predictions of the recent Flory theory of rubber elasticity. However, the small-strain theory of Langley and Graessley gave good agreement with the data. The large-strain correlations of Dossin–Graessley and Ferry–Kan did not adequately fit the data. However, the data in Figure 8 do suggest an entanglement contribution to $2C_1$ and $2C_2$. Furthermore, the values of A_3 in Figures 5 and 6 suggest an entanglement contribution to the swelling behavior as well.

Recently, Flory[37] has raised the question of whether the network connectivity, ξ, inherent in the phantom network contribution of his dual-network theory[9] should be augmented to contain an entanglement contribution. On the basis of experimental moduli extrapolated to the limit $\alpha^{-1} \rightarrow 0$ (phantom behavior), Flory[37] concluded that ξ does not contain a major contribution due to entanglements. Flory[37] tacitly took the possible enhancement of ξ by entanglements to be *independent* of strain and, therefore, concluded that entanglements do not contribute to the stress at finite strains. The values of A_2 in Figure 6 are considerably less than the corresponding values of A_1. If the magnitudes of these structure factors in excess of unity are attributed to trapped entanglements, then it would appear that the entanglement contribution to the modulus is *dependent on strain* and may disappear entirely at large elongations. Therefore, the tensile data do not contradict Flory's conclusion that entanglements *do not contribute to the phantom modulus* ($\alpha^{-1} \rightarrow 0$). However, the data strongly indicate that the finite, small-to-moderate strain modulus does contain an entanglement contribution. Therefore, a reformulation of the Flory theory accounting for the direct contribution of trapped entanglements to modulus over the entire range of strain is suggested. Such work is in progress.

Acknowledgment. These studies were supported by the C. P. Dubbs Professorship of Chemical Engineering at the Massachusetts Institute of Technology. We are grateful for helpful discussions with Professor Christopher Macosko, Department of Chemical Engineering, University of Minnesota. We also acknowledge with gratitude the cooperation of the General Electric Co., the Dow Chemical Co., and Rhône-Poulenc in providing some of the materials utilized in this study.

References and Notes

(1) K. O. Meyers and E. W. Merrill, AIChE 87th National Meeting, Boston, Mass., Aug 1979, Paper 3c.
(2) K. O. Meyers and E. W. Merrill, *Polym. Prepr., Am. Chem. Soc., Div. Polym. Chem.*, **20** (1980).
(3) W. Opperman, Sc.D. Thesis, Institute of Physical Chemistry, Technical University of Clausthal, Clausthal, West Germany, 1979.
(4) C. W. Macosko and G. S. Benjamin, *Pure Appl. Chem.*, in press.
(5) M. A. Llorente and J. E. Mark, *J. Chem. Phys.*, **71**, 682 (1979), and references therein.
(6) M. Mooney, *J. Appl. Phys.*, **19**, 434 (1948); R. S. Rivlin, *Philos. Trans. R. Soc. London, Ser. A*, **241**, 379 (1948).
(7) P. J. Flory, "Principles of Polymer Chemistry", Cornell University Press, Ithaca, N.Y., 1953.
(8) H. M. James and E. Guth, *J. Polym. Sci.*, **4**, 153 (1949).
(9) P. J. Flory, *J. Chem. Phys.*, **66**, 5720 (1977).
(10) G. Ronca and G. Allegra, *J. Chem. Phys.*, **63**, 4990 (1975).
(11) L. M. Dossin and W. W. Graessley, *Macromolecules*, **12**, 123 (1979).
(12) J. D. Ferry, "Viscoelastic Properties of Polymers", 2nd ed., Wiley, New York, 1979.
(13) W. W. Graessley, *Adv. Polym. Sci.*, **16**, 1 (1974).
(14) N. R. Langley, *Macromolecules*, **1**, 348 (1968).
(15) D. S. Pearson and W. W. Graessley, *Macromolecules*, in press.
(16) E. M. Valles and C. W. Macosko, *Macromolecules*, **12**, 673 (1979).
(17) D. S. Pearson and W. W. Graessley, *Macromolecules*, **11**, 528 (1978).
(18) C. B. Kauffman and D. O. Cowan, *Inorg. Synth.*, **6**, 214 (1969).
(19) A. L. Smith, "Analysis of Silicones", Chemical Analysis Monographs, Wiley, New York, 1974, p 152.
(20) E. A. Collins, J. Bares, and F. W. Billmeyer, "Experiments in Polymer Science", Wiley, New York, 1973.
(21) We are indebted to Dr. John Razzano of the General Electric Co., Silicones Division, for providing the 8800 and 28 100 α,ω-divinyl PDMS.

(22) We are indebted to Professor Christopher W. Macosko of the University of Minnesota, Minneapolis, Minn., for providing the Dow Corning Co. 11 100 and 21 600 α,ω-divinyl PDMS samples. Professor Macosko also performed the mercuric acetate titrations on the α,ω-divinyl PDMS.
(23) D. R. Miller and C. W. Macosko, *Macromolecules*, **9**, 206 (1976).
(24) P. J. Flory and Y. Tatara, *J. Polym. Sci.*, **13**, 683 (1975).
(25) A. L. Andrady, M. A. Llorente, and J. E. Mark, *J. Chem. Phys.*, in press.
(26) J. E. Mark, R. R. Rahalkar, and J. L. Sullivan, *J. Chem. Phys.*, **70**, 1794 (1979).
(27) D. J. Plazek, W. Dannhauser, and J. D. Ferry, *J. Colloid Sci.*, **16**, 101 (1961).
(28) N. R. Langley and J. D. Ferry, *Macromolecules*, 1, 353 (1968).
(29) The tetrafunctional cross-link was supplied by C. W. Macosko (see ref 22) and found to be 90% $[HSi(CH_3)_2O]_4Si$ by gas chromatography. The remaining 10% was assumed to be inert.
(30) Since junctions of functionality less than three are elastically ineffective, near-stoichiometric mixtures of the two network precursors were utilized in forming the tetrafunctional networks. Several suggestions have been offered as to why a stoichiometric excess of SiH groups is required to ensure complete reaction. One reason could be simple errors in measuring E_j and M_n. Another[3] is steric hindrances around the junctions requiring greater separation of chains than would be achieved with $R = 1$. A further cause could be the possible side reaction of SiH groups with ambient moisture (J. Razzano, GE Co., private communication). These points are discussed in greater detail in ref 31.
(31) K. O. Meyers, Doctoral Dissertation, Massachusetts Institute of Technology, Cambridge, Mass., 1980.
(32) The M_n given in Table II have not been corrected for w_n. Such a corrected $M_n' = (1 - w_n)M_n$. However, in the calculation of ν_s/V (using eq 17 and 18), this correction for the presence of the nonreactive oligomeric PDMS in the commercial samples was considered.
(33) J. E. Mark and J. L. Sullivan, *J. Chem. Phys.*, **66**, 1006 (1977).
(34) J. D. Ferry and H. Kan, *Rubber Chem. Technol.*, **51**, 731 (1978).
(35) M. A. Sharaf, Doctoral Dissertation, University of Cincinnati, Cincinnati, Ohio, 1979.
(36) It has been brought to our attention that the Mooney–Rivlin plots in Figure 2 do not absolutely agree with the values of $2C_1$ and $2C_2$ reported in Table IV. The Mooney–Rivlin plots in Figure 2 are the results of individual stress–strain experiments. As stated in the text, the values of $2C_1$ and $2C_2$ reported in Tables IV and V are the average of three or more such tensile experiments; therefore, there exist slight differences between Figure 2 and Table IV.
(37) P. J. Flory, *Polymer*, **20**, 1317 (1979).

Preparation and Morphological Properties of a Triblock Copolymer of the ABC Type

Yuhshuh Matsushita,* Haruhisa Choshi, Teruo Fujimoto, and Mitsuru Nagasawa

Department of Synthetic Chemistry, Nagoya University, Furo-cho, Chikusa-ku, Nagoya 464, Japan. *Received November 30, 1979*

ABSTRACT: A styrene–(4-vinylbenzyl)dimethylamine–isoprene triblock copolymer of the ABC type with a fairly narrow molecular weight distribution was prepared by an anionic polymerization method with *sec*-butyllithium in benzene. The polymerization proceeded without appreciable side reactions. The morphology of the film specimen of the triblock copolymer was investigated with electron microscopy. A clear microphase separation structure from three components was observed.

The morphology of block copolymers has been studied by various methods, but electron microscopy using an osmium tetraoxide fixation technique is the most fully developed. For example, it is well-known that the block copolymers of styrene and dienes give typical microphase separation structures[1] and the structures change with compositions of the block segments,[2] molecular weights of the polymer components,[3] casting solvents,[4] etc. Domain structures in other block copolymers have been studied and similar structures observed. However, the study of the morphology of block copolymers has been restricted to two-component systems. Although there are a few papers[6,7] on the morphology of triblock copolymers of the ABC type, clear microphase separation structures have not been observed. It seems important for the further progress in the study of polymer morphology to study triblock copolymers of the ABC type. A main goal of this work was to establish whether or not different domains can clearly be distinguished.

Block copolymers with well-defined structures can be obtained by the use of anionic polymerization methods, especially, the sequential monomer addition technique. To prepare triblock copolymers of the ABC type with relatively narrow molecular weight distributions, the experimental techniques by which monodisperse polymers can be obtained from each monomer are indispensable. Furthermore, since fractionation of mixtures of various types of copolymers is very difficult, the polymerization conditions producing only the desired block copolymer must be employed.

Preceding work has shown the conditions of polymerization of the polar monomer (4-vinylbenzyl)dimethylamine (4-VBDMA, $CH_2{=}CHC_6H_4CH_2N(CH_3)_2$) with *sec*-butyllithium in benzene to satisfy the above proposal.[8] In this work, block copolymerizations are carried out using that monomer in addition to styrene and isoprene monomers. The preparations of two kinds of diblock copolymers of the AB type consisting of polystyrene and poly(4-VBDMA) and also of polyisoprene and poly(4-VBDMA) are first studied, followed by that of triblock copolymers of the ABC type containing these three monomers.

Experimental Section

Reagents. Styrene and 4-VBDMA monomers were first dried over calcium hydride under reduced pressure and then purified by benzophenone–sodium under a pressure of ca. 10^{-6} mmHg. Isoprene was dried over calcium hydride and sodium metal and then distilled in the presence of the dipotassium salt of α-methylstyrene tetramer. The initiator, *sec*-butyllithium, was synthesized by the reaction of *sec*-butyl chloride with lithium in *n*-hexane. The concentration of initiator was determined by titration with a standard hydrochloric acid of suitable concentration. The solvents used, i.e., benzene and *n*-hexane, were

0024-9297/80/2213-1053$01.00/0